Ferretti, E., Ciccotti, M., Di Leo, A., Mulargia, F., Almagro, R., Bastianini, F.,

STATIC, DYNAMIC AND EFFECTIVE ELASTIC MODULI OF CALCARE MASSICCIO

Nota Tecnica n. 154

Anno 2004

UNIVERSITÀ DEGLI STUDI DI BOLOGNA

DISTART
Dipartimento di Ingegneria delle Strutture, dei Trasporti,
delle Acque, del Rilevamento, del Territorio

Viale Risorgimento, 2 – 40136 Bologna

Static, Dynamic and Effective Elastic Moduli of Calcare Massiccio

M. Ciccotti[1], E. Ferretti[2], A. Di Leo[2], F. Mulargia[1], R. Almagro[1], and F. Bastianini[3]

December 2, 2003

Abstract

Static and dynamic elastic moduli of *Calcare Massiccio* mudstone–limestone are measured using respectively a standard uniaxial compression test, and measurement of ultrasonic velocities. No significant frequency dependence is found for *Calcare Massiccio*, for which we measured a Young modulus of (75 ± 7) GPa and a Poisson ratio of (0.28 ± 0.02). The two techniques are also tested on a well known rheologic material providing accurate results. Finally, the effective elastic modulus is also evaluated through an identification model based on the energy dissipated during rupture. *Calcare Massiccio* is found to behave quite linearly and to develop a very low amount of damage before specimen rupture.

[1] *Dipartimento di Fisica, Settore di Geofisica, Università di Bologna,Viale Berti Pichat 8, Bologna, Italy*
[2] *DISTART, Facoltà di Ingegneria, Università di Bologna, Viale Risorgimento 2, Bologna, Italy*
[3] *Dipartimento di Ingegneria dell'Innovazione, Università di Lecce, Via per Monteroni, Lecce, Italy*

Submitted to *European Journal of Mechanics: A Solids*

1 Introduction

Elastic constants are relevant parameters whenever stresses and strains are considered. Two are the main methods used to measure them: (a) the *static method*, which is based on the measurement of the deformation induced in a material by the application of a known force; (b) the *dynamic method*, which implies measuring the ultrasonic body wave velocities. Usually, these two values do not coincide due to inelastic effects. In spite of this, the lack of available data forces one to use them indifferently, albeit with persisting doubts about the reliability of such an operation.

For what regards the Earth's crustal rocks the problem is aggravated by the fact that only dynamic measurements are readily provided by seismic waves while static measurements are possible only after extracting samples and taking them to the laboratory, an operation which is seldom possible and in all cases very expensive. As a consequence, the use of dynamic measurements in modeling is ubiquitous, yet its appropriateness is at doubt [2].

The scope of the present paper is to establish the difference in static and dynamic behavior in a compact homogeneous mudstone–limestone rock *Calcare Massiccio*, which is very interesting *per*

se because it is the typical rock of the seismic focal regions in the Apennines, central Italy [3], and for which data are totally lacking.

The static and dynamic moduli are measured using the standard techniques: uniaxial compression test, and measurement of ultrasonic velocities, which are also tested on a rheologic material, poly-methyl-methacrylate (PMMA), for which there exists a wealth of measured data at all frequencies, thus guaranteeing against systematic errors in the specific apparatuses we use.

A major difference between the static and dynamic measurements is the amplitude of the involved strains: around 10^{-7} of the dynamic measurements, up to 10^{-3} for the static ones. In the case of the static measurements on brittle materials this involves a progressive damagement of the sample from the earlier steps of the compression test. This induces a progressive alteration of the structure of the specimen making it possible to confuse material and specimen properties.

A proposal to overcome this problem has been presented by Ferretti [1]. Material properties can indeed be estracted from experimental data on the basis of an identifying model which takes into account the cross-sectional area decrement due to damage. An effective static modulus is thus determined which relates directly to the material properties.

2 Standard Methods

2.1 Dynamic Moduli

The samples of *Calcare Massiccio* were taken in the *Casavecchia Fratelli* quarry located in Cagli (Pesaro), central Italy. The chemical composition is reported in Table 1. The apparent density is $\rho = (2.71 \pm 0.03)$ kg/m^3 and the estimated porosity is $\phi = (5 \pm 2)\%$.

The high frequency moduli have been obtained by measuring the velocities v_P and v_S of longitudinal and transverse elastic waves. Isotropy was verified within experimental errors (1%) by measuring the wave velocity on a cubic sample of 10 cm side. The elastic moduli were thus calculated using the equations:

$$E = \rho \frac{v_S^2(3v_P^2 - 4v_S^2)}{v_P^2 - v_S^2} \tag{1}$$

$$\nu = \frac{v_P^2 - 2v_S^2}{2(v_P^2 - v_S^2)} \tag{2}$$

Measurements at 1 MHz have been made at EPL[1] either using two P-wave VP-1093 Pinducer transducers in transmission configuration or a single Panametrics transducer in pulse-echo configuration (V103 for P waves, V153 for S waves). Measurements at 75 kHz have only been performed for P-waves using custom transducers at the LARM laboratory. The Young modulus has been evaluated through:

$$E = \rho v_P^2 \frac{(1+\nu)(1-2\nu)}{(1-\nu)} \tag{3}$$

using the Poisson ratio measured at 1 MHz[2].

The results of the measurements on 12 prismatic *Calcare Massiccio* samples (20x5x5 cm) are reported in Table 3. It should be noted that while at 1 MHz the wavelength of 6 mm is small in relation to the sample transverse thickness, this is not the case at 75 kHz for which the wavelength is 4 cm. This could produce waveguide modes resulting in underestimates of the body wave velocity. We verified by measurements on PMMA that this does not happen because the first peak of the direct body wave is well distinguishable before the arrival of the waves reflected by the side walls. Moreover, the measurements are in accord with the preliminary measurements on the 10 cm side cubic sample.

2.2 Static Moduli

The measurement of the static elastic moduli has been performed following the standard procedure UNI9724[3] by using an AMSLER uniaxial compression machine at the LARM laboratory[4]. Following this procedure, prismatic specimens (20x5x5 cm in size) have been subjected to a low compressional displacement rate (about 0.1 mm/min), both in a monotonic load up to failure, and by several loading cycles with progressively increasing loads. The longitudinal and transverse strain in the middle cross-section have been estimated by averaging the values measured by orthogonal strain gauges (XY 91 - 6/120, produced by HBM) in the middle of the four lateral faces. The average stress on the same section has been estimated by dividing the applied load by the nominal cross-sectional area.

[1]Earthquake Physics Laboratory, Dipartimento di Fisica, Università di Bologna, Italy.

[2]The Poisson ratio is not expected to depend significantly on frequency in an isotropic medium since it is the ratio of two orthogonal deformations that should have a similar dependence on frequency.

[3]Ente Nazionale Italiano di Unificazione - http://www.uni.com - Standard norm: UNI 9724-8:1992 - ICS code: 91.100.15. Title: Stones. Determination of the elastic modulus (monoaxial).

[4]Laboratorio di Resistenza dei Materiali, Facoltà di Ingegneria, Università di Bologna, Italy.

It is important to note that the 'static' measurements are not really static since the tests have a typical duration of about 20 minutes, and have therefore associated a frequency of $\simeq 10^{-3}$ Hz – which is large in relation to tectonic loading rates.

The average stress versus strain curves for the monotonic tests on specimens C_2, C_5 and C_6 are shown in Fig. 1, the cyclic test on specimen C_1 is shown in Fig. 2. Both cases are consistent with a high degree of linearity of *Calcare Massiccio*. The values of the tangent Young modulus were determined by linearly fitting the data on a moving window and then taking the low strain limit. The results are reported in Table 2, and exhibit a small dispersion:

$$E = (77 \pm 1.5) \text{ GPa}$$

This falls within the range of compact limestones, which is comprised between 30 and 90 GPa [4] and is also consistent with the value obtained by the cyclic test. The average Poisson ratio is $\nu = (0.43 \pm 0.01)$ for the monotonic tests and (0.30 ± 0.01) for the cyclic test (see Table 2). It appears rather high for a Limestone, but this value is apparently not well constrained by this measurement technique, since the dilatancy related to the opening of small cracks induces an overestimate of the transverse strain measured at the external surface (Fettetti et al. 2003??).

We remark that the Young modulus obtained using the average longitudinal strain - i.e. the measured plate displacement divided by the specimen length - is generally 10 to 20% lower than the previous one (obtained by strain gauges). This could be due to a well known problem of the uniaxial test: notably, due to the friction on the loading plates, the contacting faces are not free to laterally expand during longitudinal compression. This implies inhomogeneous deformation with a higher strain in the central zone of the specimen. By a Finite Element simulation of this loading configuration, we verified that for an elastic material the tangent modulus - determined in the same way as in the experimental procedure described above - provides an accurate estimate of the Young modulus and Poisson ratio within 1%.

The difference must then be imputed to the inevitable damage of the external edges of the specimen near the loading plates, which results in a local weakening of the material and in a change in its structural behavior. For this reason it is advisable to measure the local strain in the central region of the specimen which is both undamaged and uniformly stressed (Ferretti et al., 200???). A method to takle with these problems is described in next section.

3 Effective static moduli

The object in testing is never the material, but a small structure interacting with the test-machine. Thus, experimental results univocally characterize the behavior of the specimen-test machine system. The present section will describe the derivation and application of an identifying model that allows to separate the material properties from the evolution of the structural properties of the sample.

3.1 Generalities on the identifying model of the effective law

The identifying model adopted here has been developed on concrete in order to tackle with the non-objectiveness of the standard approach in front of the size-effect and to investigate the physical origin of strain-softening, i.e. the decline of stress at increasing strain. In fact, in the standard approach, strain-softening is associated with a phase of material instability which has questionable physical meaning. On the basis of the relationship between v_P and E (Eq. 3), strain-softening was considered as an unacceptable feature for a constitutive equation [6], since the longitudinal wave speed, v_P, ceases to be real if E becomes negative. Moreover, it has been questioned [7, 8, 9, 10] whether strain-softening in a continuum is a sound concept from the mathematical point of view. The question was whether or not strain-softening is a real material property or merely the result of inhomogeneous deformation caused by experimental techniques (cf. [11] and references therein).

The new proposal was inspired by the argumentations from Hudson et al. [5] concerning the implications of the failure mechanism on the specimen response. It was assumed that strain-softening is due to scaling the applied force by the original cross-sectional area rather than the actual cross-sectional area - named the "resistant area" A_{res} (Fig. 4b) - as it happens with steel subjected to traction (Fig. 4a). Since the resistant area decrement is an internal not observable mechanism in concrete and in brittle rocks, the function $A_{res} = A_{res}(\varepsilon)$ is not directly measurable and has to be identified by a model. In Fig. 4b, qualitative effective laws are provided for three different assumptions on A_{res}.

We now illustrate the details of the model by showing its original application on concrete specimens where the effects are magnified. The load-displacement curves and the classic average stress versus average strain relationships for the experimental acquisitions on cylinders with variable H/R ratio are provided in Figs. 5 and 6.

In accordance with the identifying model of the effective law [1], we evaluate an effective stress:

$$\sigma_{eff} = \frac{N}{A_{res}} = \overline{\sigma}\frac{A_n}{A_{res}}. \tag{4}$$

where N is the applied load, $\overline{\sigma}$ is the average stress, and the resistant area A_{res} is related to the nominal area A_n in accordance with the Fracture Mechanics with Damage:

$$A_{res} = A_n\,(1 - D)\,. \tag{5}$$

where the damage parameter D is a scalar comprised between 0 (test begin) and 1 (crushing). However, while in the Fracture Mechanics with Damage D is considered as a material property, here D is considered as a structural property, due to the propagation of cracks in the specimen and it is experimentally evaluated calculating the quantity:

$$D = W_d / W_{d,t} \tag{6}$$

where W_d is the dissipated energy at the current point and $W_{d,t}$ is the total dissipated energy. To evaluate W_d at a given point, we unload the specimen and evaluate the area below the load-displacement curve as shown in Fig. 7.

Since it can be experimentally appreciated that damage does not evolve during the unloading-reloading cycles, the resistant area does not change and the unloading-reloading slope E_s characterizes the instantaneous stiffness of the material as a function of the average strain. We can thus define an effective strain

$$\varepsilon_{eff} = \sigma_{eff}/E_s \tag{7}$$

as shown in Fig. 8 along with the identified $\sigma_{eff} - \varepsilon_{eff}$ relationships.

The average curve in Fig. 8 is actually a monotone non-decreasing one, as it was expected from the preventive theoretical analysis (Fig. 4b). This is a notable result, since the monotonicity of the effective law has not been assumed a-priori. Moreover, since the dispersion range in Fig. 8 is very narrow, it can be stated that the $\sigma_{eff} - \varepsilon_{eff}$ curves are size-effect insensitive. It can also be shown [12] that the identified curve is not sensitive to changes of failure mechanism.

Numerical simulations of the structural behavior have shown how the monotone effective law can provide results in good agreement with the experimental data [1], even in triaxial compressive loading [11].

3.2 Application to Calcare Massiccio

We now apply the identifying model of the effective law to the cyclic test performed on specimen C_1 whose $\overline{\sigma} - \overline{\varepsilon}$ plot is shown in Fig. 2.

The interpolated slope of the unloading-reloading cycles (see Fig. 9) is shown to be substantially constant (within a few %) with the increasing average strain. It can thus be concluded that the instantaneous stiffness of the material does not substantially change during loading. That is, we can consider with good approximation that *Calcare Massiccio* behaves as a linear elastic material up to failure.

The evolution of the resistant area A_{res} as a function of the average strain, evaluated by means of Eqs. (6) and (5) and by the knowledge of the unloading-reloading law, turned out to be very weak (see Fig. 10). This means that in Calcare Massiccio the gap between structural and material behavior is very little. We can thus expect an effective law very close to the average law as shown in Fig. 11, with σ_{eff} given by Eq. (4).

The tangent effective Young modulus for the cyclic test on the specimen C_1 turned out to assume the value $E_{eff} = 68$ GPa. Since the resistant area is very close to the nominal area until crushing, the assumption of no-damage and uniform stress on the middle cross-section is well accurate in *Calcare Massiccio*. This results in a reliable evaluation of the material stiffness provided by strain-gauge acquisitions on the middle cross-section.

4 Discussion

The measured static Young modulus of Calcare Massiccio, $E = (77 \pm 1.5)$ GPa ($E_{eff} = 68$ GPa) is lower than the dynamic value, $E = (81 \pm 5)$ GPa, as it is generally espected, but the two measurements turn out to be substantially consistent within experimental errors and sample variability.

To investigate the accuracy of the experimental methods we used the same techniques and apparatuses on a well known material, PMMA[5], for which a wealth of measurements exists and

[5]We used cast PMMA (Plexiglas) produced by Röhm and Haas Italia Srl

which, being a rheologic material, exhibits a large variation between static and dynamic moduli.

The stress-strain diagrams are reported in Fig. 3. The static measurements gave a value of $E = (3.6 \pm 0.1)$ GPa and a Poisson ratio $\nu = 0.38$. The dynamic measurements gave a constant value of $E = (6.0 \pm 0.2)$ GPa at both 75 kHz and 1 Mhz with a Poisson ratio $\nu = 0.33$. While the dynamic values are very stable and highly consistent with independent measurements, with E ranging between 6.0 and 6.3 GPa and $\nu = 0.33$ [13, 14, 15], it is difficult to state the accuracy of the measurements at lower frequency. The Young modulus of PMMA appears in many reference tables which routinely do not specify the measurement technique. The most common value is comprised between 3 and 3.2 GPa [13, 16, 17], but the reported range is between 2.7 GPa [18, 19] and 3.7 GPa [20]. As an exception, Koppelmann [21] provided a complete curve of the Young modulus of PMMA for frequencies ranging from 10^{-4} to 10^{3} Hz, suggesting a static limit $E = 3$ GPa, then a progressive rise with frequency up to 5 GPa at 1 kHz where the trend is still positive. The Poisson ratio is fairly constant at $\nu = 0.33$ except for a drop to 0.30 near the maximum slope of the Young modulus.

It is typical to find an unresolvable 10 to 20% bias between different measurement techniques. While the large frequency dependence of the Young modulus of PMMA is in any case well apparent, this is not the case for non rheologic materials like *Calcare Massiccio*. In this case there is no evidence of a frequency dependence on the elastic moduli and the use of the dynamic method appears to provide both the easiest and the most accurate values, especially for the Poisson ratio.

For the purpose of geophysical modeling we can thus retain a unique value for the Young modulus of *Calcare Massiccio* $E = 75$ GPa, and consider a typical error bar of $\pm 10\%$ which comprises our dynamic, static and effective estimates performed at room temperature over nine decades in frequency. For the Poisson ratio we should retain the dynamic estimate $\nu = 0.28 \pm 0.02$.

The good accordance between the static-dynamic and effective analysis gives generality and further validation to the identification model of the effective law, which has been settled on concrete. When identifying the constitutive law, this model allows us to take into account the resistant area decrement due to damage. This results in average and effective stress-strain laws no more homothetic, in general. In particular, the effective law is always monotone, even if the experimental load-displacement diagram is softening. For this model, the gap between average and effective behavior is expected to vanish in linear elastic materials, since damage is negligible in these ma-

terials. To verify this statement, the identifying model has been tested on Calcare Massiccio, a material traditionally assumed as linear elastic. A poor developing of damage has been actually found in Calcare Massiccio, following in effective laws close to the average ones. In such a type of material, there is a negligible decrement of resistant area and the difference between effective and dynamic elastic moduli is very small.

Finally, from Figs. 7 and 10, it may be concluded that the failure mechanism is very different in concrete-like and rock-like materials. Actually, the identifying model of the effective law returns a sensitivity of the damage/resistant area to the load step which is relevant in concrete-like materials (Fig. 7) and negligible in rock-like materials (Fig. 10). This results in a failure mechanism with propagation of macro-cracks from the very beginning of the compression test forth, for concrete-like materials, and a failure mechanism without significant damage evolution up to crushing, for rock-like materials.

Acknowledgments

This work was supported by the GNV project Poseidon and @DISTART?. Special thanks to R. Carli, L. Pasquini, and S. Castellaro for important contribution in the measurement process.

References

[1] Ferretti E. Modellazione del comportamento del cilindro fasciato in compressione, Ph.D. Thesis, 2001.

[2] Jaeger JC, Cook NGW. Fundamentals of rock mechanics. London: Chapman and Hall, 1969.

[3] Almagro R. Caratterizzazione meccanica di un litotipo sismico italiano: il Calcare Massiccio, Graduate thesis, 2002.

[4] Carmichael RS. Handbook of physical properties of rocks, CRC Press, Inc., Vol. III, 1984.

[5] Hudson JA, Brown ET, Fairhurst C. Shape of the Complete Stress-Strain Curve for Rock, 13th Symposium on Rock Mechanics, 1971.

[6] Hadamard J. Leons sur la Propagation des Ondes (Chapter VI), Paris: Hermann et Cie, 1903.

[7] Bergan PG. Record of the Discussion on Numerical Modeling, IUTAM W. Prager Symposium, Northwestern University, Evanston, Ill., 1983.

[8] Hegemier GA, Read HE. Some Comments on Strain-Softening, DARPA-NSF Workshop, Northwestern University, Evanston, Ill., 1983.

[9] Sandler I, Wright JP. Summary of Strain-Softening, DARPA-NSF Workshop, Northwestern University, Evanston, Ill., 1983.

[10] Ferretti E. Discussion on Strain-Softening in Concrete, submitted to International Journal of Fracture, letters in fracture and micromechanics, 2003.

[11] Ferretti E, Di Leo A. Modeling of Compressive Tests on FRP Wrapped Concrete Cylinders through a Novel Triaxial Concrete Constitutive Law, SITA, 2003, 5, pp. 20–43.

[12] Ferretti E, Bastianini F. Identification of the Local Law for Concrete Cylinders under Uniaxial Monotone Compression, ABDM Symposium, full test on CD, 2002.

[13] Boudet JF, Ciliberto S. Interaction of sound with fast crack propagation. Phys. D, 2000, 142, pp. 317–345.

[14] Filippi P, Habault D, Lefebvre JP, Bergassoli A. Acoustics: basic physics theory and methods, Academic Press, 1999.

[15] Ferry JD. Viscoelastic properties of polymers. New York: J.Wiley & Sons, 1980.

[16] Fineberg J, Gross SP, Marder M, Swinney HL. Instability in dynamic fracture. Phys. Rev. Lett., 1991, 67, pp. 457–460.

[17] Niemann G. Elementi di Macchine. Edizioni di Scienza e Tecnica Milano. Springer-Verlag Berlin, 1981.

[18] Williams JG, Radon JC, Turner CE. Designing against fracture in brittle plastics. Polym. Eng. and Sci., April 1968, pp. 130–141.

[19] Barquins M, Petit JP. Kinetic instabilities during the propagation of a branch crack: effects of loading conditions and internal pressure. J. of Struct. Geol., 1992, 14, pp. 893–903.

[20] Enciclopedia dell'Ingegneria. Istituto Editoriale Internazionale. Arnoldo Mondadori Editore. Vol. I, 1971.

[21] Koppelmann VJ. Über die Bestimmung des dynamischen Elastizitätsmoduls und des dynamischen Schubmoduls im Frequenzbereich von 10^{-5} bis 10^{-1} Hz. Rheologica Acta, 1958, 1, pp. 20–28.

Table captions

Table 1

Chemical composition of *Calcare Massiccio* obtained through XRF analysis at the Dipartimento di Scienza della Terra of Bologna, Italy. *LOI* stands for *Loss On Ignition*.

Table 2

Static elastic moduli for the monotonic tests on the three specimens C_2, C_5 and C_6, and the cyclic test on specimen C_1.

Table 3

Measured P and S waves velocities and dynamic moduli evaluated through (1) and (2) when v_S is available, or otherwise through (3) with ν assumed to be the same as the one measured at 1 MHz. The P wave velocity 1 MHz is the average value between pulse-echo and transmission measurements, which differed only by 0.6%.

CaO	50,55%
LOI	43,69%
MgO	5,00%
Fe_2O_3	0,30%
Al_2O_3	0,20%
Sr	170 ppm
Trace Elements	0.24%

Table 1: Chemical composition of *Calcare Massiccio* obtained through XRF analysis at the Dipartimento di Scienza della Terra of Bologna, Italy. *LOI* stands for *Loss On Ignition*.

	S mm^2	E_l GPa	E_t GPa	ν
C_2	107.0	78.4	-180	0.43
C_5	120.7	77.0	-179	0.43
C_6	109.1	75.3	-173	0.44
mean	112	77	-178	0.43
std	7	1.5	4	0.01
C_1	87.5	78.8	-260	0.30

Table 2: Static elastic moduli for the monotonic tests on the three specimens C_2, C_5 and C_6, and the cyclic test on specimen C_1.

f (kHz)	v_P (m/s)	v_S (m/s)	E (GPa)	ν
1000	6195 ± 150	3427 ± 90	81.4 ± 4.5	0.28 ± 0.02
75	6169 ± 260	-	80.7 ± 7	-

Table 3: Measured P and S waves velocities and dynamic moduli evaluated through (1) and (2) when v_S is available, or otherwise through (3) with ν assumed to be the same as the one measured at 1 MHz. The P wave velocity 1 MHz is the average value between pulse-echo and transmission measurements, which differed only by 0.6%.

Figure captions

Figure 1

Stress-strain diagrams for the monotonic test on specimens C_2, C_5 and C_6. The straight line represents an estimate of the tangent modulus in the low strain limit.

Figure 2

Stress-strain diagram for the cyclic test on specimen C_1. The straight line represents and a linear fit in the whole cycled region.

Figure 3

Stress-strain diagram for the monotonic (dashed) and cyclic (solid) test on PMMA specimens C_2 and C_1. The straight lines represent estimates of the tangent moduli in the low strain limit.

Figure 4

Stress identification from load data: influence of the middle cross-section evaluation for steel (a) and concrete (b).

Figure 5

Size effect for the load-displacement diagrams: concrete specimens.

Figure 6

Size effect for the average stress versus average strain diagrams: concrete specimens.

Figure 7

Evolution of resistant area and damage law for concrete specimens with variable H/R ratio. The inlet shows the evaluation of the dissipated energy W_d.

Figure 8

$\sigma_{eff} - \varepsilon_{eff}$ dispersion range for variable H/R ratio and average curve: concrete specimens. The inlet shows the identification of the effective strain ε_{eff}: the generic point $\sigma_{eff} - \varepsilon_{eff}$ results from the intersection of the two lines $\sigma = \sigma_{eff}$ and $\sigma = E_s\varepsilon$.

Figure 9

Interpolating law of unloading-reloading slope versus average strain for Calcare Massiccio.

Figure 10

Percentage resistant area versus average strain for Calcare Massiccio.

Figure 11

Comparison between the average and effective law for Calcare Massiccio.

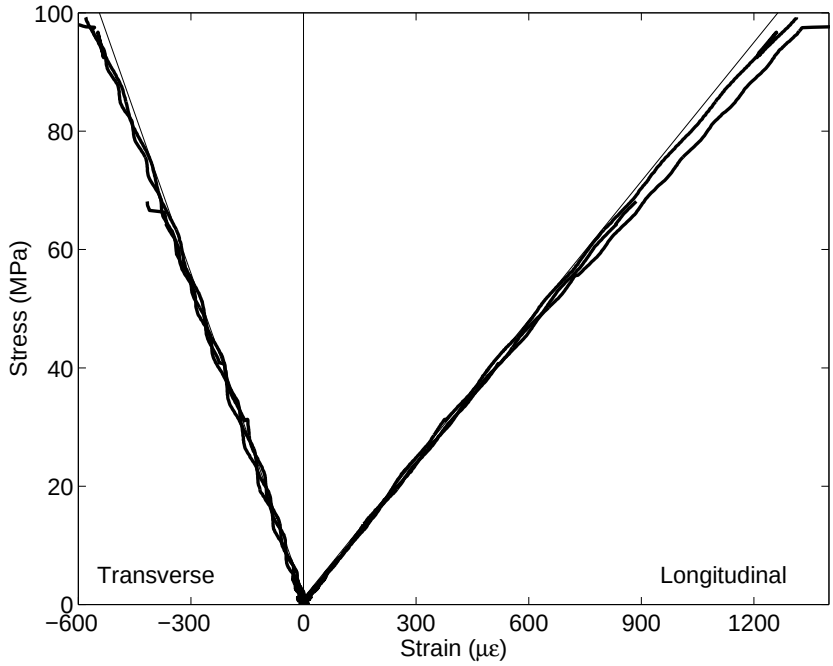

Figure 1: Stress-strain diagrams for the monotonic test on specimens C_2, C_5 and C_6. The straight line represents an estimate of the tangent modulus in the low strain limit.

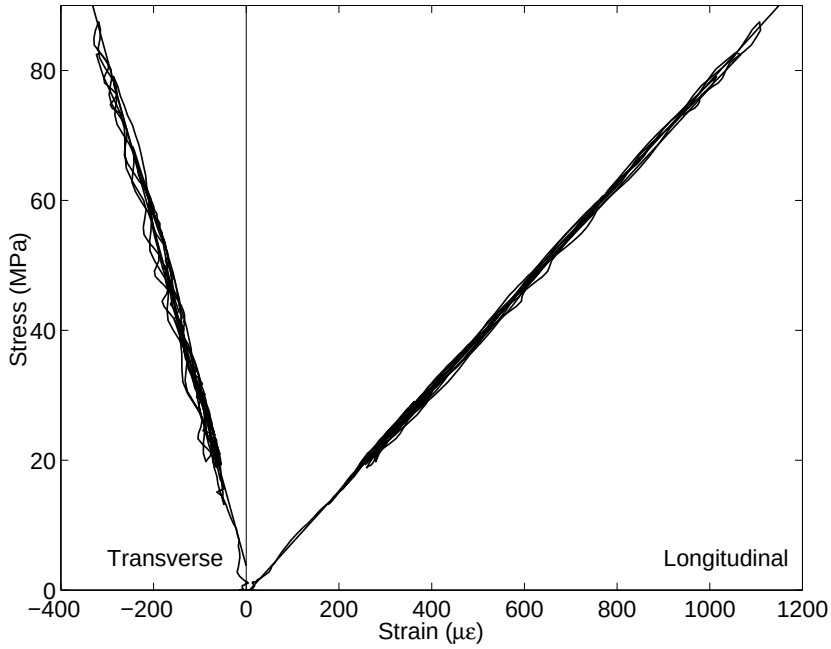

Figure 2: Stress-strain diagram for the cyclic test on specimen C_1. The straight line represents and a linear fit in the whole cycled region.

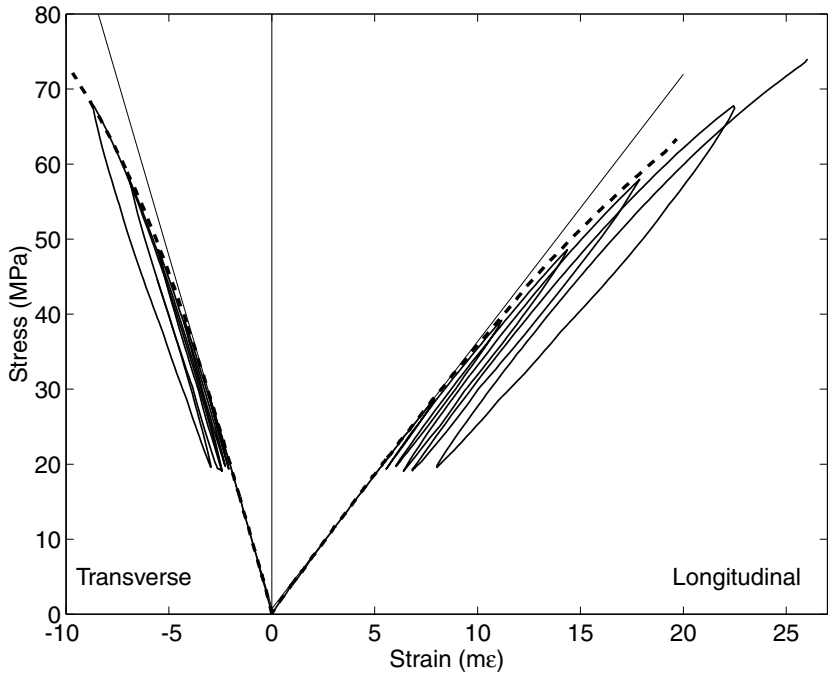

Figure 3: Stress-strain diagram for the monotonic (dashed) and cyclic (solid) test on PMMA specimens C_2 and C_1. The straight lines represent estimates of the tangent moduli in the low strain limit.

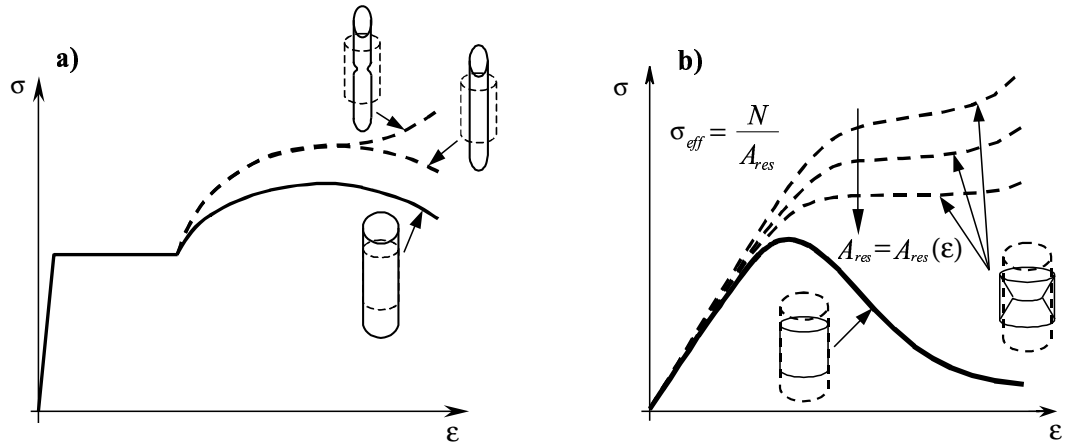

Figure 4: Stress identification from load data: influence of the middle cross-section evaluation for steel (a) and concrete (b).

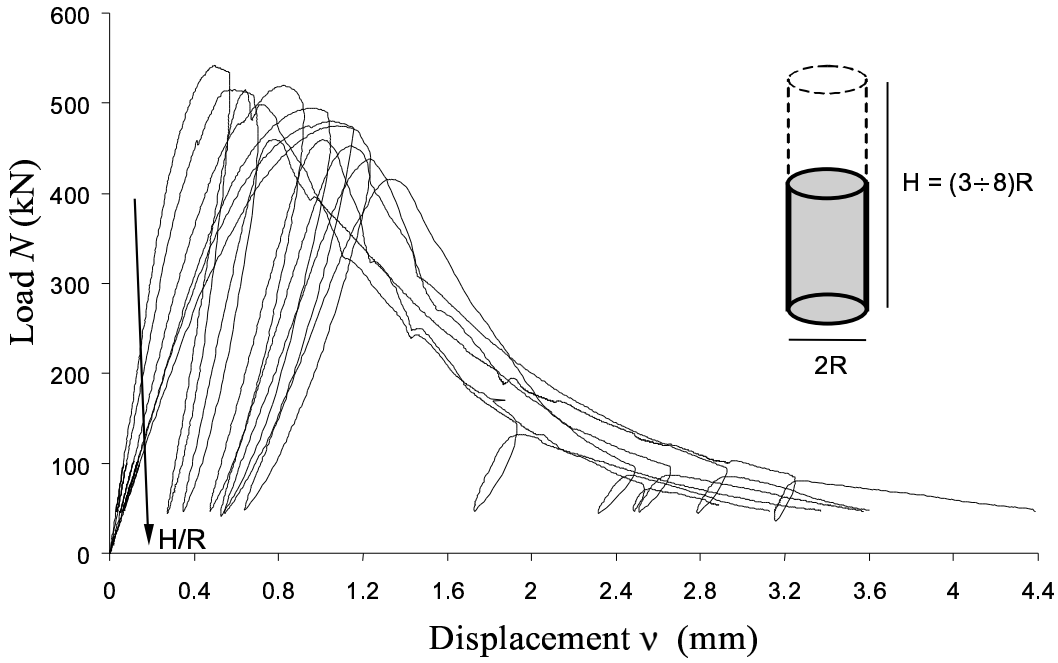

Figure 5: Size effect for the load-displacement diagrams: concrete specimens.

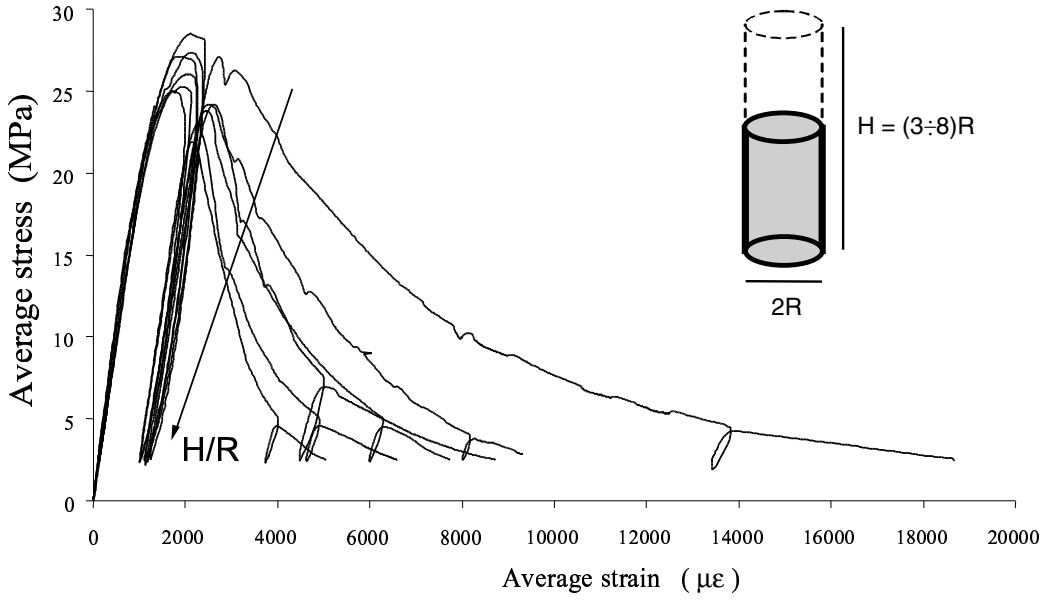

Figure 6: Size effect for the average stress versus average strain diagrams: concrete specimens.

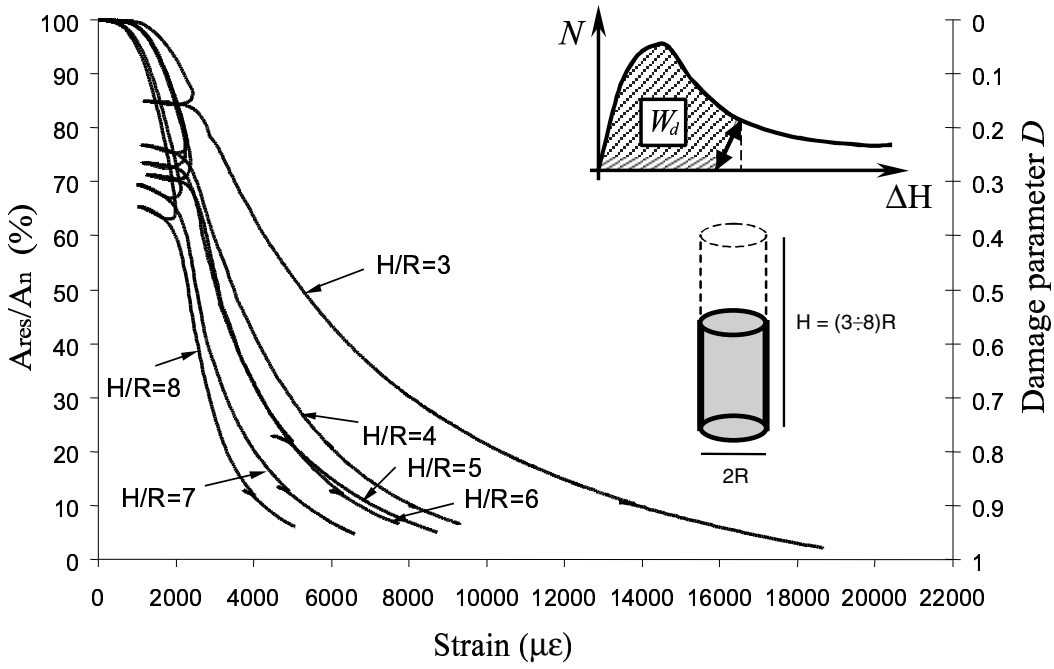

Figure 7: Evolution of resistant area and damage law for concrete specimens with variable H/R ratio. The inlet shows the evaluation of the dissipated energy W_d.

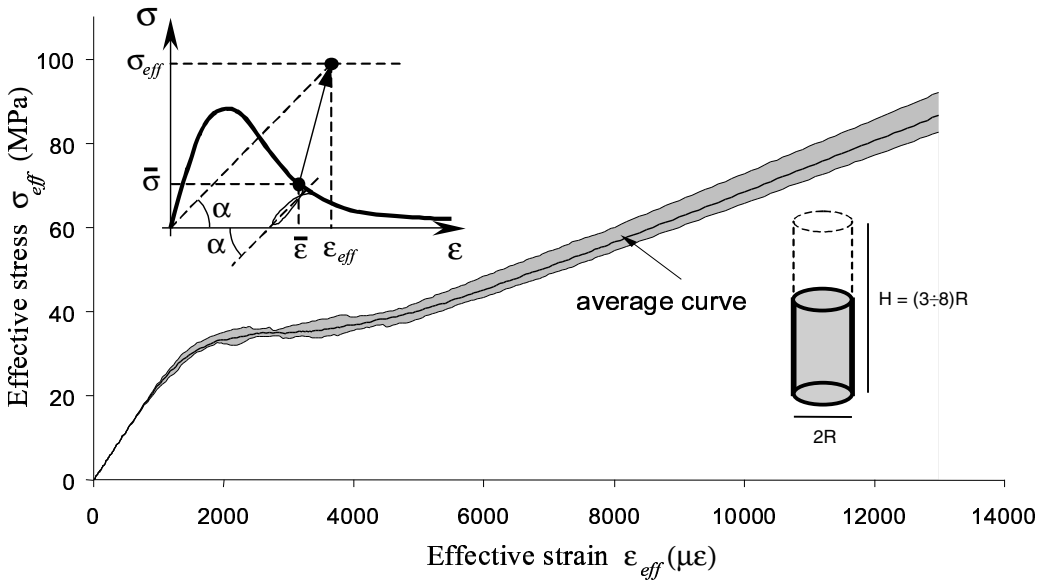

Figure 8: $\sigma_{eff}-\varepsilon_{eff}$ dispersion range for variable H/R ratio and average curve: concrete specimens. The inlet shows the identification of the effective strain ε_{eff}: the generic point $\sigma_{eff}-\varepsilon_{eff}$ results from the intersection of the two lines $\sigma=\sigma_{eff}$ and $\sigma=E_s\varepsilon$.

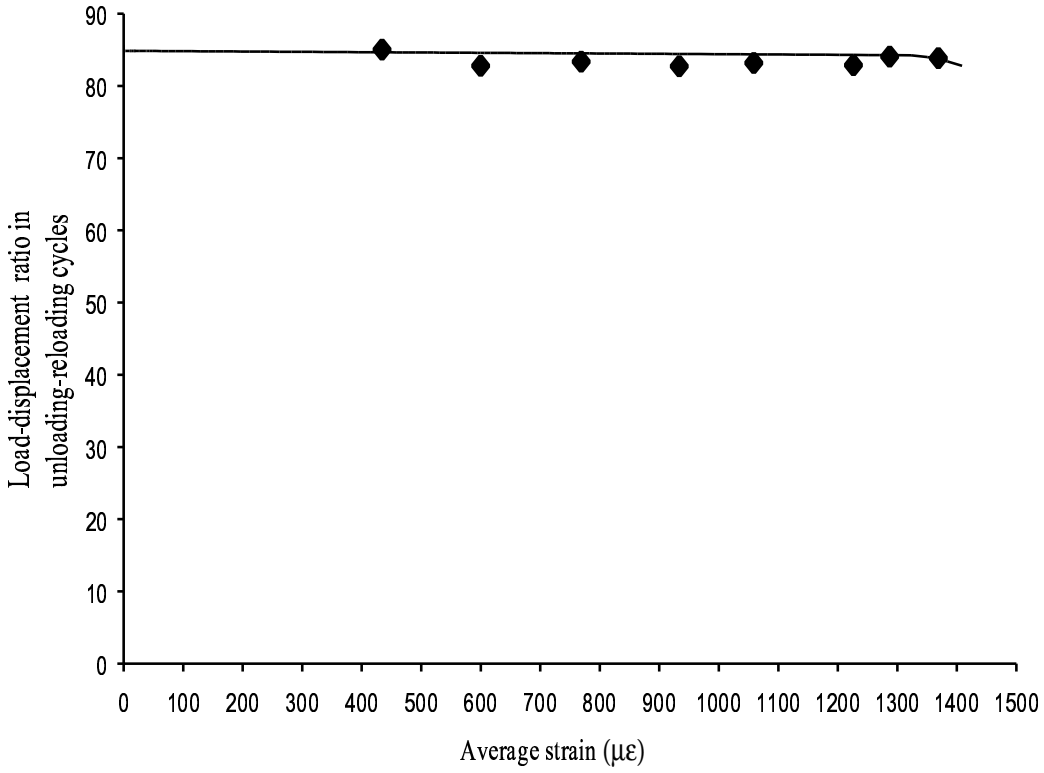

Figure 9: Interpolating law of unloading-reloading slope versus average strain for Calcare Massiccio.

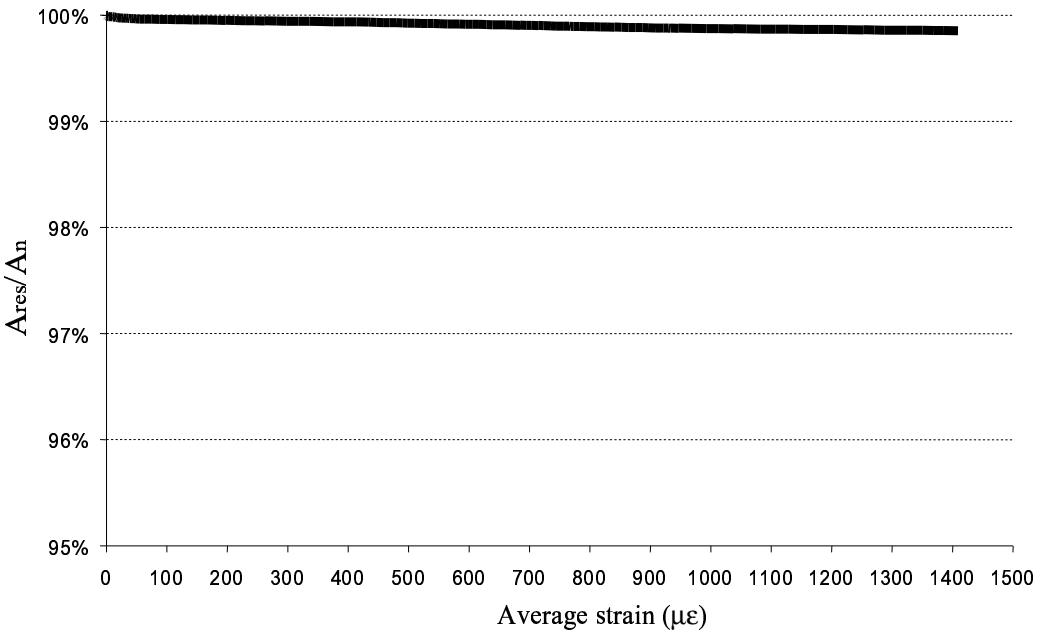

Figure 10: Percentage resistant area versus average strain for Calcare Massiccio.

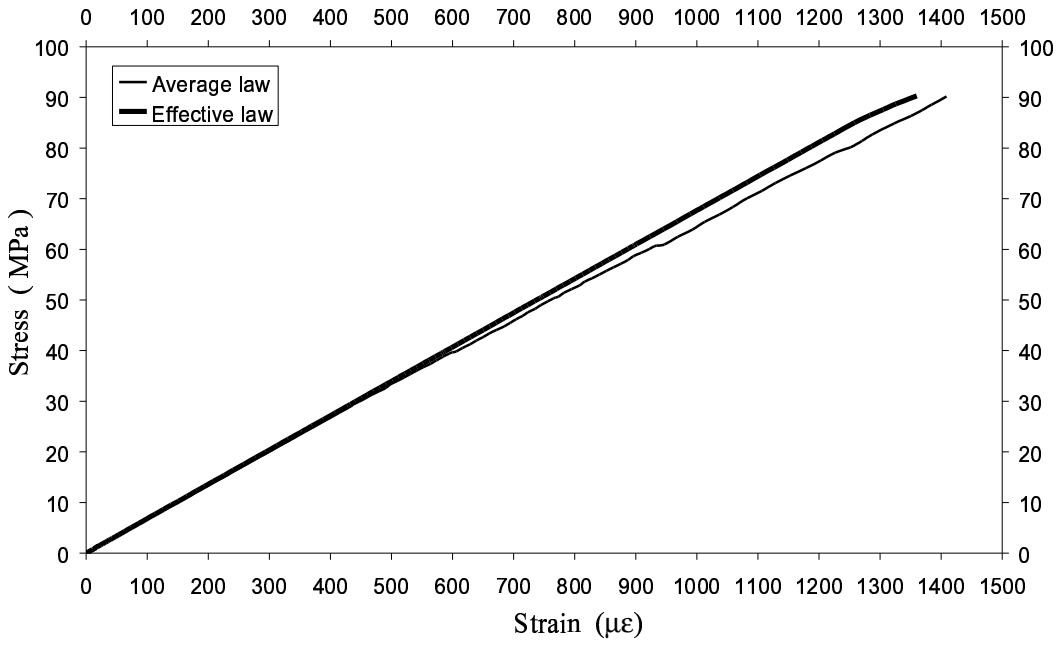

Figure 11: Comparison between the average and effective law for Calcare Massiccio.